Construction of C/MoS_2 nanocomposite for highly efficient electrocatalytic NRR

Yang Guohua[1,*], *Li Nan*[2]

[1,2] School of Materials Science and Engineering, Jilin University, Changchun, Jilin, 130012, P. R. China

Abstract. Electrochemical N_2 reduction reaction (NRR) has been considered as a promising and green process to replace conventional Haber−Bosch process. However, the presence of sluggish reaction kinetics and competitive hydrogen evolution reaction (HER) can result in poor activity and unsatisfactory selectivity. Here, we proposed C/MoS_2 catalysts by a facile 'one-pot' hydrothermal method. Benefiting from porous nanosphere structure, it shows outstanding charge transfer rate, which accelerates NRR kinetics. As a result, C/MoS_2 exhibited a conspicuously improved NRR performance with a high Faradaic efficiency (FE) of 8.2% at −0.7 V. In addition, this electrocatalyst showed marvelous stability.

1 Introduction

NH_3, a critical nitrogen building block for production of fertilizers, and plastics, can also be a promising carbon-free energy carrier in future energy industry. At present, the traditional Haber-Bosch process for industrial ammonia production is not only energy-intensive, but also leads to serious environmental pollution. Therefore, it is of paramount importance to explore an economic and sustainable alternative to achieve efficient ammonia production.[1–3]

The ambient electrocatalytic N_2 reduction reaction (NRR) represents a promising alternative for clean and energy-saving NH_3 production. Unfortunately, to date, NRR has been obstructed by lacking of efficient electrocatalysts. On the one hand, NRR is less likely to occur than the simultaneous hydrogen evolution reaction (HER), thus leading to the restricted selectivity. On the other hand, a large overpotential is usually needed.[4,5] Therefore, developing suitable catalyst with high selectivity at a low overpotential is a significant part to realize efficient NRR process.[6] Noble-metal-based catalysts (Ru, Au, etc.) are considered to be the most effective electrocatalysts due to their high intrinsic activity, but their widespread use is restricted by low abundance and high cost. [4,7] It is thus highly desired to design and develop non-precious metal alternatives. MoS_2 nanosheets offered great interest towards NRR because of high surface area, optimized N_2 absorption energy and tunable electronic structure. [8,9]However, because of its poor conductivity, which greatly inhibits charge transfer rate, MoS_2 displays low NRR catalytic activity. [10] To meet this challenge, the introduction of conductive carbonaceous materials, such as graphene, carbon nanotubes, have been proven to be particularly effective.[11] However, most of reported methods have been hampered by complicated steps required to prepare the carbon nanostructures themselves.[12]

Herein, we reported a C/MoS_2 nanocomposite as effective NRR catalyst by a facile one-pot hydrothermal method. Obviously, our synthesis strategy is easier to handle than those using prefabricated carbon materials. In addition, because of its unique nanostructure, the rate of charge transfer is greatly accelerated, which is beneficial to NRR. As a result, C/MoS_2 nanocomposite presented a largely enhanced NRR activity.

2 Experimental section

2.1 Synthesis of electrocatalysts

The synthesis of C/MoS_2 nanospheres was based on a previous procedure with modifications. Typically, 0.6 g of sodium molybdate (Na_2MoO_4), 3 g of thiourea (CH_4N_2S) and 1 g of polyvinyl pyrrolidone (PVP) were dissolved in 30 mL deionized water with magnetic stirring to form a uniform solution. Then, we added 0.2 g of dopamine hydrochloride (DPH) into the above mixture with forming a red suspension. After continuously stirring for 30 min, the resulting suspension was put into a 50-mL Teflon-lined stainless steel autoclave kept at 200 °C for 18 h, followed by cooling down to room temperature naturally. The black precipitates were collected and washed with deionized water and absolute ethanol by centrifugation method, and dried under vacuum at 60 °C for overnight. Lastly, C/MoS_2 nanospheres were obtained by the calcination of black precipitates in argon atmosphere at 700 °C for 3 h.

2.2 Electrochemical measurements

All electrochemical experiments were performed in a three-electrode system using CHI660E electrochemical workstation with N_2-saturated (purity: 99.999%) 0.1 M

* Corresponding author: a17808082580@163.com

Li_2SO_4 in a two-compartment cell separated by Nafion 211 membrane. Polarization curves were measured with a scan rate of 5.0 mV s^{-1} at room temperature. The concentrations of NH_3 produced were determined by the indophenol blue method and N_2H_4 as the possible by-product was detected by the method of Watt and Chrisp. Before NRR measurement, the electrolyte was pre-saturated with high-purity N_2 (purity: 99.999%) for 30 minutes with a flow rate of 50 standard cubic centimeter per minute (sccm). In this work, all measured potentials (vs. Ag/AgCl) were transformed into the potentials vs. reversible hydrogen electrode (RHE) based on the equation: $E_{RHE} = E_{Ag/AgCl} + 0.059\ pH + E^{o}_{Ag/AgCl}$

3 Results and Discussion

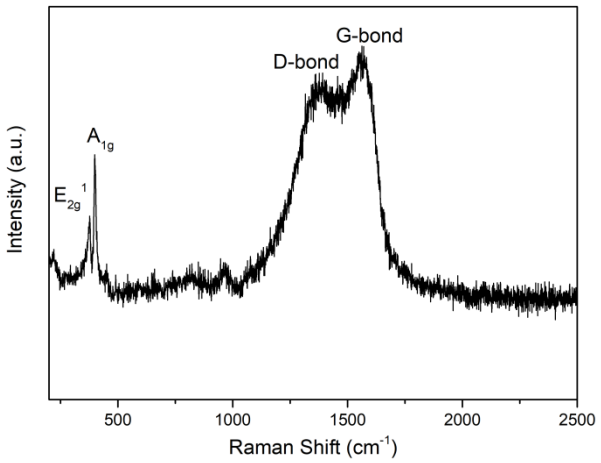

Fig.1. Raman spectra of C/MoS_2

As shown in Fig.1, two peaks at ~376 and 402 cm^{-1} are attributed to in-plane $E_{2g}{}^1$ and out-of-plane A_{1g} vibrational mode, respectively, confirming MoS_2 structure. The other two characteristic peaks located at 1373 cm^{-1} (D band) and 1605 cm^{-1} (G band) belong to the carbon phase. The calculated intensity ratio between D band and G band is 0.87, indicating that carbon shows a higher degree of graphitization. Therefore, the raman spectroscopy proves coexistence of MoS_2 and carbon phase.[13]

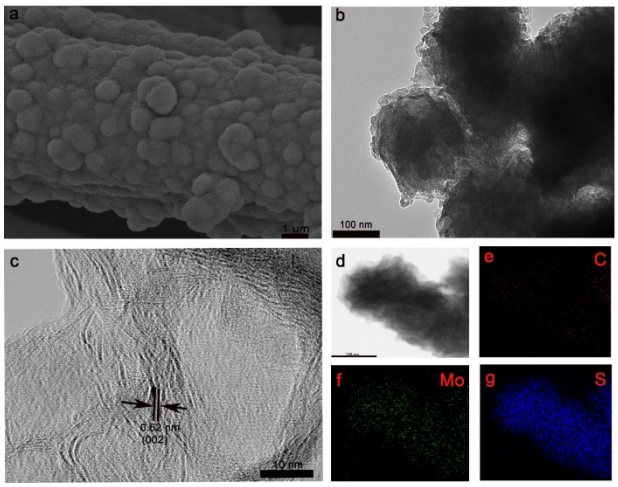

Fig.2. (a) SEM image of C/MoS_2; (b) TEM image of C/MoS_2 (c) HRTEM images of C/MoS_2; (d)-(g) HAADF-STEM image of C/MoS_2 and corresponding elemental images of C, Mo, and S.

Fig.2a shows that C/MoS_2 is of porous nanospheres nanostructure assembled from ultra-thin C/MoS_2 nanosheets. Figure 2b further reveals that nanosheets are covered with a thin carbon layer and are in close contact with each other to form nanospheres. Such open porous structure facilitates electronic contact and rapid electron transfer during catalytic process. The HRTEM image in Fig. 2C clearly shows lattice fringe of 0.62 nm consisting with (002) crystal planes of MoS_2. From Figure 2d, EDX mapping images were also demonstrated a uniform distribution of C, Mo and S elements in the entire C/MoS2.[14]

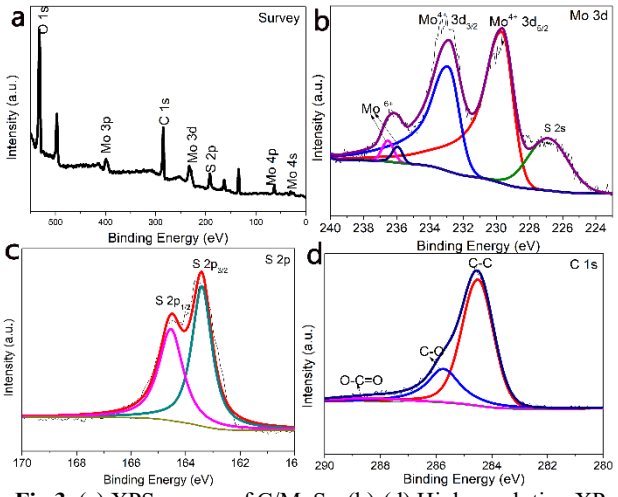

Fig.3. (a) XPS survey of C/MoS_2; (b)-(d) High-resolution XP spectra of C/MoS_2; (b) Mo 3d region; (c) S 2p region; (d) C 1s region.

Figure 3a presents survey spectrum of C/MoS_2, revealing the presence of Mo, S, C and O elements in the sample, where the signal of O originates from surface oxidation. The high-resolution Mo 3d XPS spectrum in Fig. 3b can be classified into two pairs, corresponding to Mo^{4+} of MoS_2 (232.8 and 229.8 eV) and Mo^{6+} (235.9 and 236.6 eV) configurations. The peak at 226.9 eV is assigned to the S 2s. The appearance of Mo^{6+} structures in samples stem from the inevitable air contact. As seen from the high-resolution spectra of the S 2p region (Fig. 3c), the S 2p spectrum of C/MoS_2 can be deconvoluted into two peaks. The doublet at 163.4 and 164.6 eV is assigned to the S $2p_{3/2}$ and $2p_{1/2}$ of S^{2-} in MoS_2. Figure 3d shows C 1s high-resolution XPS spectra of C/MoS_2. As for C/MoS_2, the C 1s band can be fitted to three peaks, attributable to O-C=O (288.7 eV), C–O (285.8 eV) and C-C (284.6 eV).[15–17]

4 Electrochemistry performance

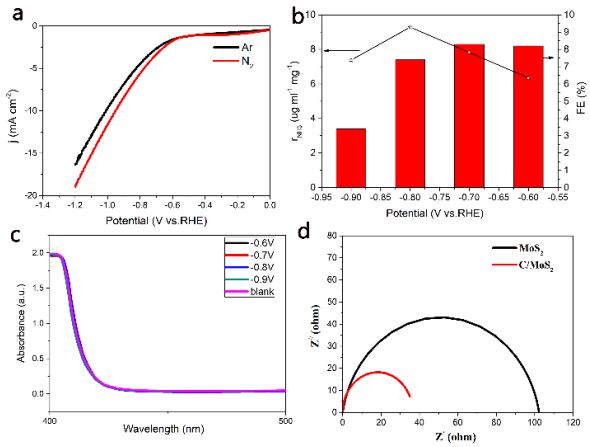

Fig.4. (a) LSV curves of C/MoS_2 obtained from Ar- and N_2-saturated 0.1 M Li_2SO_4 electrolytes using a scan rate of 5 mV s^{-1}; (b) Average yield rates of ammonia and Faradic efficiency at each given potential; (c) UV-Vis absorption spectra of N_2H_4 solution; (d) Nyquist plots of C/MoS_2 and pure MoS_2.

LSV curve shows a distinct current enhancement below −0.6 V under a N_2 atmosphere (Fig. 4a). As observed in Fig 4b, the highest FE of 8.2 % is obtained at -0.7 V. It is worth noting that we failed to detect N_2H_4 (Fig 4c), which manifests that C/MoS_2 shows excellent selectivity for NH_3 formation. In addition, the electrochemical impedance spectroscopy (EIS) was performed in Fig. 4d to analyze electron transfer properties brought by Carbon. It can be seen that the charge transfer resistance (R_{ct}) of C/MoS_2 (38 Ω) was smaller than pure MoS_2 (104 Ω), demonstrating that the synergetic effect of C and MoS_2 can effectively regulate the electronic structure of C/MoS2, bringing about the faster electron transfer process that boosts the reaction kinetics for NRR.

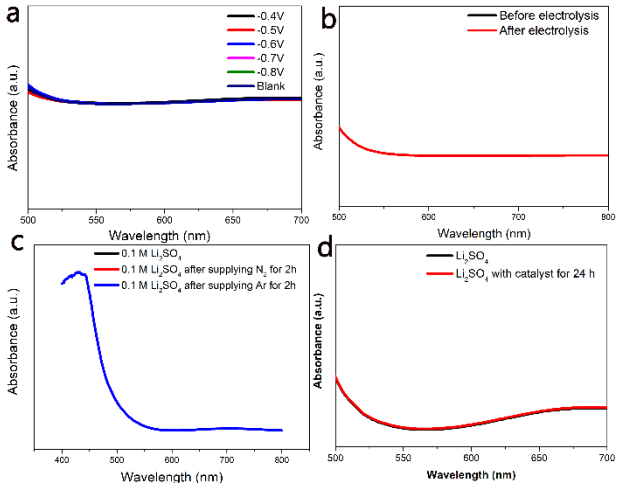

Fig.5. (a) UV-Vis absorption spectrum under Ar saturated Li_2SO_4 solution; (b) UV-Vis absorption spectrum under open circuit voltage; (c) excluding the interference of ammonia gas in the air; (d) UV-Vis absorption spectra of electrolyte soaked by C/MoS_2 for 24h.

The absorbance curve after electrolysis in Ar almost coincides with the curve without electrolysis, proving that no NH_3 is produced in electrolysis under Ar environment (Fig. 5a). Meanwhile, we separately performed electrolysis in N_2-saturated solution under an open circuit potential at −0.7V for 2 h. As a result, no NH_3 was found, which more accurately confirmed that N_2 was the only source of NH_3 production(Fig. 5b). Considering that there may be a small amount of NH_3 in the air, we keep the high-purity gases (Ar and N_2, purity: 99.999%) flowing in the sealed electrolyte without applying voltage, and the corresponding UV-Vis absorption spectrum shows that NH_3 is not detected, indicating that it does not come from the atmosphere interference with gas supply. (Fig. 5c)No NH_3 was detected in electrolyte with C/MoS_2 catalyst immersed for 24 h, which eliminates possible influence of N element attached to the surface of catalyst (Fig.5d). The above control experiments ensure the accuracy of the experimental results.

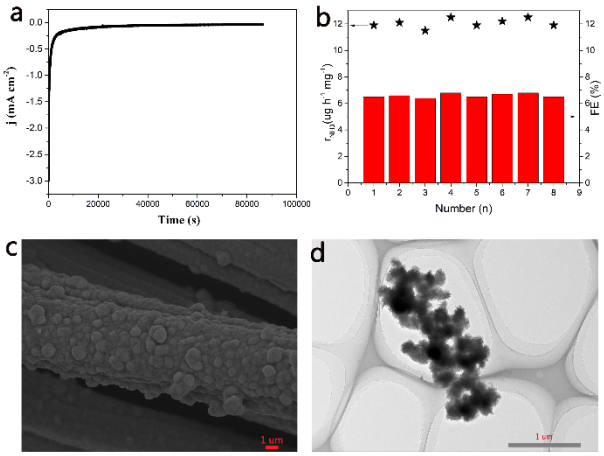

Fig. 6 stability test of C/MoS_2 (a) i-t curve of 20 hours (b) 8 cycles of tests (c) SEM and (d) TEM of C/MoS_2 after 16 hours' electrolysis.

After 20 h of electrolysis, C/MoS_2 presents no pronounced degradation in charge density, proving the excellent long-term stability of C/MoS_2 (Fig.6a). In Fig.6b, such catalyst was tested at -0.7 V for eight times. Both the NH_3 average and FE hardly decline during consecutive recyclingate tests, indicating it has exciting stability. After stability test, the resulting C/MoS_2 was collected and further analyzed by SEM and TEM. Remarkably, C/MoS_2 still keeps its primary morphology (Fig. 6c,d), demonstrating the outstanding structural stability.

5 Conclusion

In conclusion, we utilized C/MoS_2 nanocomposite by a facile hydrothermal method for NRR. Benefiting from porous nanospheres structure, C/MoS_2 nanosheets provide a fast path for charge transfer and maintain the high stability and conductivity. Therefore, C/MoS_2 displays excellent FE and remarkable stability. Our findings open up a new avenue for the design of active and stable electrocatalysts towards NRR.

Reference

1. P. Chen, N. Zhang, S. Wang, T. Zhou, Y. Tong, C. Ao, W. Yan, L. Zhang, W. Chu, C. Wu, Y. Xie, *Proc Natl Acad Sci U S A* **2019**, *116*, 6635–6640.
2. P. Song, H. Wang, L. Kang, B. Ran, H. Song, R. Wang, *Chem Commun* **2019**, *55*, 687–690.
3. H. Nan, Y. Liu, Q. Li, P. Shen, K. Chu, *Chem. Commun.* **2020**, *56*, 10345–10348.
4. D. Liu, M. Chen, X. Du, H. Ai, K. H. Lo, S. Wang, S. Chen, G. Xing, X. Wang, H. Pan, *Adv. Funct. Mater.* **2020**, *2008983*, 1–36.
5. F. Wang, X. Lv, X. Zhu, J. Du, S. Lu, A. A. Alshehri, K. A. Alzahrani, B. Zheng, X. Sun, *Chem Commun* **2020**, DOI 10.1039/c9cc09803h.
6. W. Guo, K. Zhang, Z. Liang, R. Zou, Q. Xu, *Chem Soc Rev* **2019**, *48*, 5658–5716.
7. H. Du, X. Guo, R. M. Kong, F. Qu, *Chem Commun* **2018**, *54*, 12848–12851.
8. H. Zhang, C. Cui, Z. Luo, *J. Phys. Chem. C* **2020**, *124*, 6260–6266.
9. B. H. R. Suryanto, D. Wang, L. M. Azofra, M. Harb, L. Cavallo, R. Jalili, D. R. G. Mitchell, M. Chatti, D. R. MacFarlane, *ACS Energy Lett.* **2018**, *4*, 430–435.
10. C. S. L. Koh, H. K. Lee, H. Y. Fan Sim, X. Han, G. C. Phan-Quang, X. Y. Ling, *Chem. Mater.* **2020**, *32*, 1674–1683.
11. X. Li, X. Ren, X. Liu, J. Zhao, X. Sun, Y. Zhang, X. Kuang, T. Yan, Q. Wei, D. Wu, *J. Mater. Chem. A* **2019**, *7*, 2524–2528.
12. N. Li, Z. Liu, Q. Gao, X. Li, R. Wang, X. Yan, Y. Li, *J. Mater. Sci.* **2017**, *52*, 13183–13191.
13. J. Chen, G. Liu, Y. Zhu, M. Su, P. Yin, X. Wu, Q. Lu, C. Tan, M. Zhao, Z. Liu, W. Yang, H. Li, G. H. Nam, L. Zhang, Z. Chen, X. Huang, P. M. Radjenovic, W. Huang, Z. Q. Tian, J. F. Li, H. Zhang, *J Am Chem Soc* **2020**, DOI 10.1021/jacs.0c01649.
14. H. Li, Y. Zhao, C.-A. Wang, *J. Mater. Sci. Mater. Electron.* **2018**, *29*, 13703–13708.
15. X. Hu, X. Zeng, Y. Liu, J. Lu, S. Yuan, Y. Yin, J. Hu, D. T. McCarthy, X. Zhang, *Appl. Catal. B Environ.* **2020**, *268*, DOI 10.1016/j.apcatb.2019.118466.
16. Y. Zhang, M. Shi, C. Wang, Y. Zhu, N. Li, X. Pu, A. Yu, J. Zhai, *Sci. Bull.* **2020**, *65*, 359–366.
17. H. Wu, H. Jile, Z. Chen, D. Xu, Z. Yi, X. Chen, J. Chen, W. Yao, P. Wu, Y. Yi, *Micromachines (Basel)* **2020**, *11*, DOI 10.3390/mi11020189.